

Comparative and verified studies of zirconium nanocomposite nanofibres by bubble spinning

Ya Li¹, Ji-Huan He^{1,2} ✉

¹National Engineering Laboratory for Modern Silk, College of Textile and Clothing Engineering, Soochow University, 199 Ren-Ai Road, Suzhou 215123, People's Republic of China

²Jiangsu Wangong Technology Group Co., Ltd., Suzhou, People's Republic of China

✉ E-mail: hejihuan@suda.edu.cn

Published in Micro & Nano Letters; Received on 10th April 2017; Revised on 25th July 2017; Accepted on 12th October 2017

Zirconia nanocomposite nanofibres were prepared from several different as-spun fibre polymers fabricated by the bubble spinning, a novel spinning method for mass production of nanofibres. To obtain various zirconia nanocomposites, several polymers were used as zirconia powder carriers for a bubble spinning. The morphology, the thermal/mechanical property and pore-size distribution of the obtained nanofibres were characterised and the theoretical fluid mechanics analyses were described, then a comparative and verified study drew a conclusion on the distinctions of their principle structural diagrams, resulting in different properties. Among all these nanocomposites, PAN-based zirconia nanocomposite was found to outperform all the rest nanocomposites, which had the best thermal stability, the most uniform pore structure and the highest strength.

1. Introduction: Zirconia is well known for its high temperature resistance and heat insulating properties due to its high melting point of about 2700°C. Therefore, zirconia fibres have been intensively investigated for thermal insulating applications to take the advantage of fibre form induced anisotropic thermal conductivity [1, 2]. In recent years, nanofibres have attracted great attention for their wide ranges of potential applications such as filtration, sensors, drug delivery, biomedical, protective clothing, catalysis, energy storage and generation due to their large surface area and abundant active surface, superior physical and mechanical properties [3–6]. Zirconia nanofibre mats are believed to have a better thermal resistance property than conventional fibre mats for their extremely high porosity brought by the nanoscale dimension of the fibres. Electrospinning is a simple method for producing nanofibres [7]. Zhang and Edirisinghe [8] prepared zirconia nanofibres by calcination of electrospun zirconia composite nanofibres using a polymer blend of polyoxyethylene and polyethylene glycol (PEG) (weight ratio 1:2) as the carrier media. Lamastar *et al.* [9] fabricated poly(vinyl alcohol)/zirconia nanofibres with an average diameter of 600 nm. However, the low output of electrospinning severely limits the industrial applications of electrospun nanofibre. To solve this problem, bubble spinning was recently invented using polymer bubbles for mass production of nanofibres [10, 11].

Bubble spinning is to use polymers' or melts' bubbles for fabrication of nanomaterials, which includes smooth and discontinuous nanofibres by using electrostatic force, blowing air or mechanical force to overcome the surface tension. It provides the best candidate for mass production of nanofibres. The ejection velocity in the bubble spinning process can be as high as 100 m/s, and the spinning process can be finished within 0.001 s, the minimal diameter of the obtained fibre can be as small as 5 nm. Besides, the morphologies by bubble spinning can be controlled by different kinds of methods for various applications.

To investigate the feasibility of mass production of zirconia nanofibres, this Letter prepared several zirconium nanocomposite nanofibres using bubble spinning. Through the comparison of the morphology, the thermal/mechanical property and pore-size distribution, which were in order to evaluate the potential applications of zirconia nanofibres, several polymers were used as zirconia powder carriers by bubble spinning were studied, besides, the mechanical property and pore-size distribution of the obtained

nanofibres were also verified by theoretical fluid mechanics analyses to find the relationship.

2. Experimental details: 0.5 g polyvinylpyrrolidone was dissolved in 0.4 g deionised water, then 0.5 g zirconia was added to the solution followed by magnetic stirring over 24 h to obtain a zirconia suspension. PEG was then added to the suspension as a dispersant. Finally, the zirconia suspension was mixed with pre-prepared 13% poly(vinylidene-fluoride)/N,N-dimethylformamide (PVDF/DMF), 13% nylon 66 (PA66), formic acid, 13% polyacrylonitrile/N,N-dimethylformamide (PAN/DMF) and 13% poly(styrene)/N,N-dimethylformamide (PS/DMF) solutions, respectively, for spinning.

Each polymer solution was transferred to the solution reservoir of a bubble-spinning setup for electrospinning. The schematic of bubble-spinning setup is shown in Fig. 1. The applied voltage was set at 25 kV and the collecting distance was kept 15 cm. The composite fibres were collected on aluminium foil to form non-woven mats. All spinning processes were carried out under ambient conditions. All electro-spinning processes were carried out under ambient conditions. When the roller rotated, the bubble, under the electronic force, was broken, and then multiple jets were formed, which were received on the collector above as nanofibres. Another bubble was produced when the adjacent hole reached its top, so the motor could exactly control the frequency of the bubble formation. The optical image of bubble jets was also shown as below. All the collected samples were placed in a vacuum oven for 24 h at room temperature to remove the solvent residuals.

The surface morphology of the zirconia composite fibres was examined by field emission scanning electron microscope (SEM, Hitachi-S4800, Hitachi, Japan). To characterise the thermal decomposition profiles, TGA was performed on a Diamond TG/DTA 5700 (PerkinElmer, USA). The tensile properties of all samples were characterised with a universal electromechanical test machine (Instron-3365, Instron Corporation, USA). The dimensions of the tensile test specimens were 50 mm (*L*) × 10 mm (*W*) × 0.2 mm (±0.01 mm) (*T*). Qualitative analysis of porosity of the nanofibre mats was performed using through-pore size analyser (Porometer 3G, Quantachrome Instruments, USA). X-ray diffraction (XRD) patterns were obtained using a Rigaku D/Max 2400/PC diffractometer (Japan) with Cu K α radiation

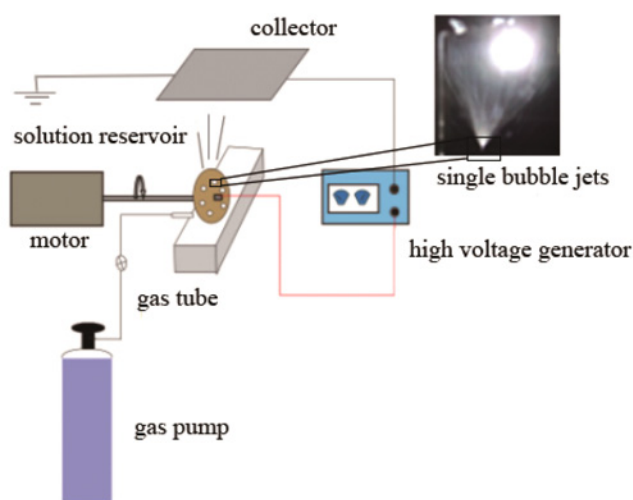


Fig. 1 Device for bubble spinning

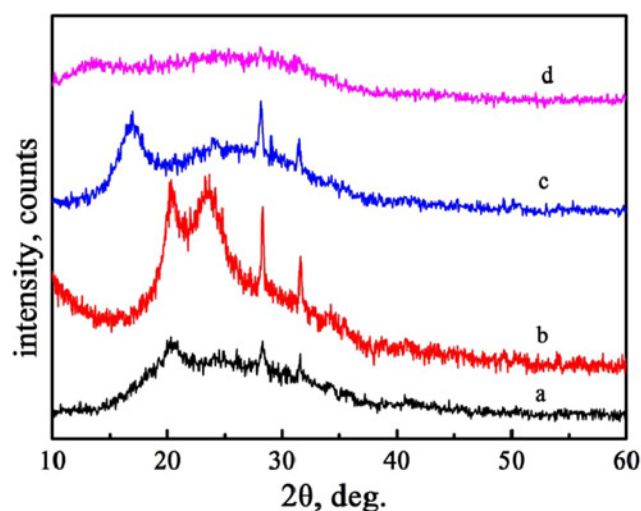


Fig. 2 XRD patterns of different zirconium nanocomposite nanofibres
a PVDF/DMF with zirconia
b PA66/formic acid with zirconia
c PAN/DMF with zirconia
d PS/DMF with zirconia

($\lambda = 0.154$ nm) in a 2θ range from 10° to 60° . The measurements were repeated three times, respectively, for each sample.

3. Results and discussion: XRD spectra of the precursor fibres were presented in Fig. 2. The obvious diffraction peaks located at $2\theta = 28.6^\circ$ and 31.7° corresponding to (1–11) and (111) planes indicated the presence of single monoclinic phase (JCPDS Card No. 34-0104). It demonstrated that different polymers based zirconia nanocomposite nanofibres were successfully fabricated via bubble spinning.

The four structural morphologies of the fabricated nanofibres were shown in Fig. 3. Nanocomposite zirconia nanofibres were proved formable from all the employed polymers but fibre diameters varied due to the varying solution viscosity induced by the different polymer molecular structures. Besides, the average fibre diameters of the four types of nanocomposite zirconia nanofibres were presented in Table 1.

Fig. 4 shows the thermal behaviour of pre-oxidised zirconia nanocomposite nanofibres. Weight loss of all samples started at about 400°C . The weight losses of zirconia/PA66 and zirconia/PS were sharp and loss of about 80% of their weight at below 600°C . Zirconia/PVDF experienced a slower decomposition starting at

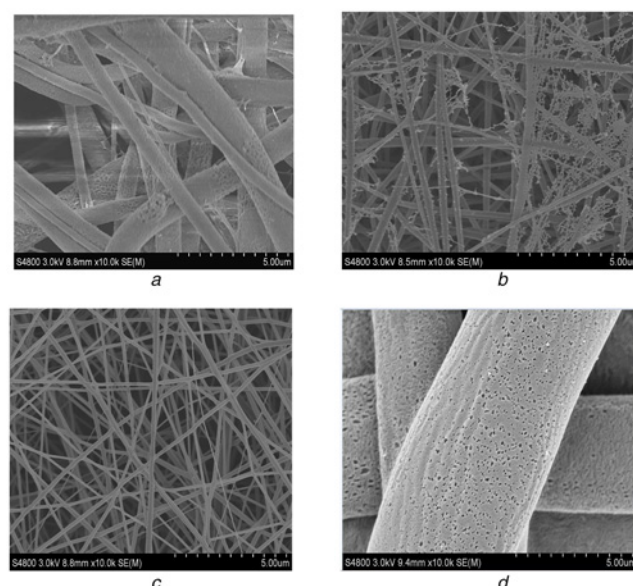


Fig. 3 FE-SEM micrograph of fibres from different zirconium nanocomposite nanofibres

a PVDF/DMF with zirconia
b PA66/formic acid with zirconia
c PAN/DMF with zirconia
d PS/DMF with zirconia

Table 1 Average diameters of different zirconium nanocomposite nanofibres

Parameter	PVDF/ DMF/ZrO ₂	PA66/formic acid/ZrO ₂	PAN/DMF/ ZrO ₂	PS/DMF/ ZrO ₂
average diameter, nm	673.12	232.51	163.05	4807.62

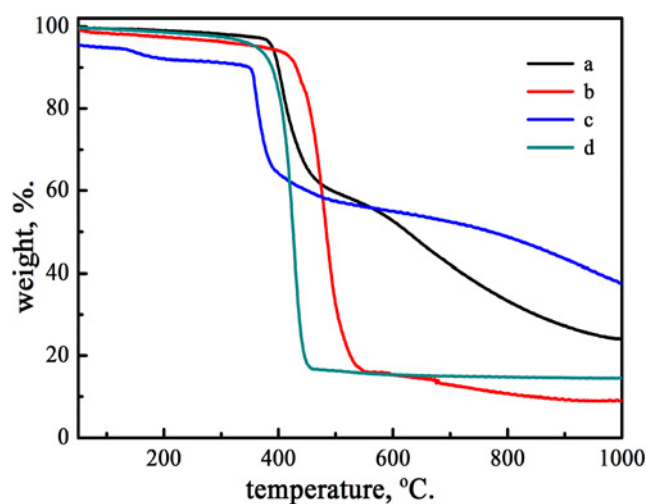


Fig. 4 TG-DTA curves of electrospun nanocomposites with varying ratios of polymers

a PVDF/DMF with zirconia
b PA66/formic acid with zirconia
c PAN/DMF with zirconia
d PS/DMF with zirconia

around 500°C but retained around 30% weight till 1000°C . PAN experienced a carbonisation process in nitrogen during the thermal analysis process. Due to the previous pre-oxidation of the ladder type molecular chain had a certain supporting function of the fibres, and then the decomposition was not dominant. It had a

quality reducing process in the removal of N/O/H/ and so on between 100 and 400°C, however, the velocity was quite slow in relative terms. Then from 400 to 600°C, PAN started to decompose, meanwhile intermolecular crosslinking reaction and fibre carbonisation happened, generating the amorphous carbon. Afterwards amorphous carbon turned into graphite crystal at higher temperatures, so the amount tended to be stable during 600–1000°C. It can be clearly seen that there were about 40% remaining, containing ZrO₂ and graphite crystals, which indicated the thermal stability of zirconia/PAN/DMF was better than the others.

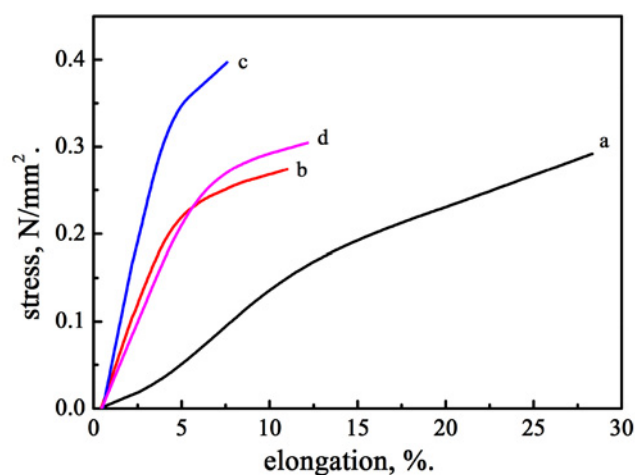


Fig. 5 Elongation at break of different zirconia nanocomposite nanofibre
a PVDF/DMF with zirconia
b PA66/formic acid with zirconia
c PAN/DMF with zirconia
d PS/DMF with zirconia

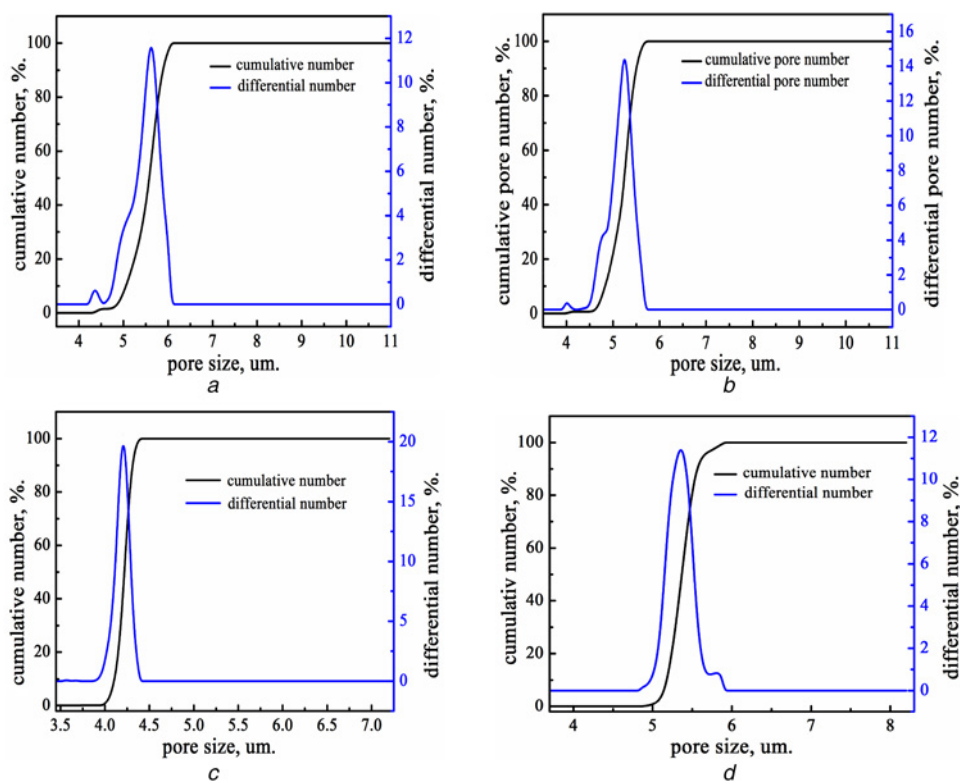


Fig. 6 Pore sizes of different zirconium nanocomposite nanofibres
a PVDF/DMF with zirconia
b PA66/formic acid with zirconia
c PAN/DMF with zirconia
d PS/DMF with zirconia

Fig. 5 shows the stain–stress curves of the four nanocomposite nanofibre mats. At least five measurements for each sample were performed in the testing. It can be seen that the elongation at break of the PVDF composite mats was 28.26% when the strength at break of PAN composite mats reached 0.394 N/mm², it was noteworthy that the strength of PAN-based zirconia nanofibre membrane was the strongest while the PVDF-based zirconia nanofibre membrane was the most elastic one.

Fig. 6 shows the pore-size distribution of each nanofibre mat. It could be seen that a majority of the pores in PAN-based zirconia nanofibre membrane had a pore size smaller than 4.5 µm, while the pore sizes of the rest zirconia nanofibre membranes were mostly larger than 5 µm. The pore-size distribution of PAN-based zirconia nanofibre membrane was also the most uniform. This might be one of the explanations of the higher strength of PAN-based zirconia nanofibre membrane [12].

Then from the morphology, the mechanical property and pore-size distribution of the obtained nanofibres, the great connection was found. Owing to the testing theories and methods of machines (Instron-3365 and Porometer 3G), pressure changes under mechanical tensile and aerodynamic force were different for these four zirconia nanocomposite nanofibres, they can be divided into four simple principle structural diagrams displayed in Fig. 7.

Fig. 7c shows that PAN composite nanofibres' surfaces were uniform and smooth, their diameters were the smallest while the tensile strength was the biggest, meanwhile pressure change after infiltration under aerodynamic force was little, then the porosity was small and even. The average diameter of PS composite fibres was the biggest as thick as 4.8 µm, there were some pores nearly the same sizes as shown in the principle structural diagram of Fig. 7d, the tensile strength was medium while pressure change after infiltration under aerodynamic force was the most, so the porosity was the biggest. Grooves on PVDF composite nanofibres' rough surfaces were in different sizes and they would be deformed along the

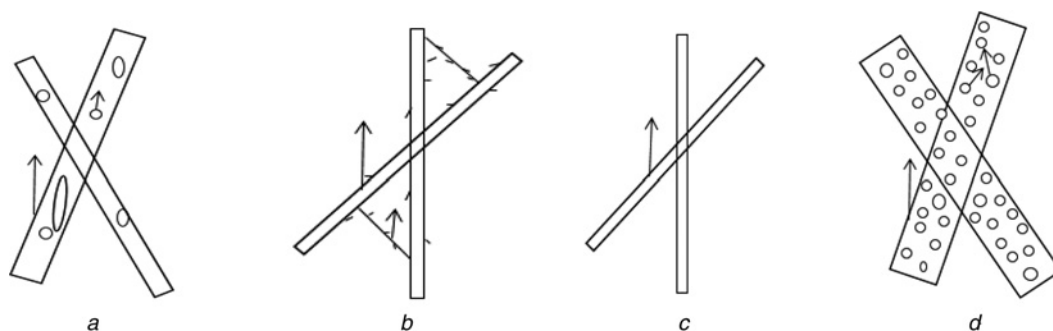


Fig. 7 Simple principle structural diagrams of different zirconia nanocomposite nanofibres
 a PVDF/DMF with zirconia
 b PA66/formic acid with zirconia
 c PAN/DMF with zirconia
 d PS/DMF with zirconia

directions of forces easily, so the tensile strength was the smallest, just as shown in Fig. 7a. In comparison, PA66 composite nanofibres in the principle structural diagram of Fig. 7b were smooth and their diameters were small, but some adhesions existed between fibres, and then the tensile strength and the porosity were both media. Therefore, among all these nanocomposites, PAN-based zirconia nanocomposite was found to outperform all the rest nanocomposites, which had the highest tensile strength and the most uniform pore structure. Then the structures and the test results were verified to be consistent.

4. Conclusion: Different polymers based zirconia nanocomposite nanofibres were successfully fabricated via bubble spinning and it demonstrated the feasibility of mass production of zirconia nanocomposite nanofibres. The diameters of the nanofibres were measured varying from around 50 to 5000 nm.

To investigate the potential application of the fabricated zirconia nanocomposite nanofibres, the morphology, the thermal/mechanical property and pore-size distribution of the obtained nanofibres were characterised and the theoretical fluid mechanics analyses were described. A comparative and verified study drew a conclusion on the distinctions of their principle structural diagrams, resulting in different properties. It showed that PAN-based zirconia composite nanofibre mat had the most uniform diameter, the smallest average pore size and the most uniform pore structure, the highest strength and the most stable thermal resistant properties, which implied that bubble-electrospun PAN-based zirconia composite nanofibre mat could be a promising material.

5. Acknowledgments: This work was supported by National Natural Science Foundation of China (grant no. 11372205 and 51403143), Six Talent Peak of Jiangsu Province (grant no. ZBZZ-035), Research and Innovation Project for College Graduates of Jiangsu Province (grant no. KYLX16_0135) and it has been sponsored by China Scholarship Council.

6 References

- [1] Khajavi R., Abbasipour M.: 'Electrospinning as a versatile method for fabricating coreshell, hollow and porous nanofibers', *Sci. Iran*, 2012, **19**, (6), pp. 2029–2034
- [2] Esfandarani M.S., Johari M.S.: 'Producing porous nanofibers'. In Proceedings of the 2nd Int. Conf. on NANOCON, Olomouc, Czech Republic, EU, 2010, **10**, pp. 1–6
- [3] Lee Y.S., Ji S.I.: 'Preparation of functionalized nanofibers and their applications', in Kumar A. (Ed.): 'Nanofibers' (InTech, Winchester, UK), 2010, pp. 438
- [4] Niemann M.U., Srinivasan S.S., Phani A.R., *ET AL.*: 'Nanomaterials for hydrogen storage applications: a review', *J. Nanomater.*, 2008, **2008**, (1), pp. 145–152
- [5] Shuakat M.N., Lin T.: 'Recent developments in electrospinning of nanofiber yarns', *J. Nanosci. Nanotechnol.*, 2014, **14**, (2), pp. 1389–1408
- [6] Farajpour M.R., Rastgoo A., Farajpour A., *ET AL.*: 'Vibration of piezo-electric nanofilm-based electromechanical sensors via higher-order non-local strain gradient theory', *Micro Nano Lett.*, 2016, **11**, (6), pp. 302–307
- [7] Cui X.M., Nam Y.S., Lee J.Y., *ET AL.*: 'Fabrication of zirconium carbide (ZrC) ultra-thin fibers by electrospinning', *Mater. Lett.*, 2008, **62**, (12–13), pp. 1961–1964
- [8] Zhang H.B., Edirisinghe M.J.: 'Electrospinning zirconia fiber from a suspension', *J. Am. Ceram. Soc.*, 2006, **89**, (89), pp. 1870–1875
- [9] Lamastar F.R., Bianco A., Meriggi A., *ET AL.*: 'Nanohybrid PVA/ZrO₂ and PVA/Al₂O₃ electrospun mats', *Chem. Eng. J.*, 2008, **145**, (1), pp. 169–175
- [10] He J.H., Kong H.Y., Yang R.R., *ET AL.*: 'Review on fiber morphology obtained by bubble electrospinning and blown bubble spinning', *Therm. Sci.*, 2012, **16**, (16), pp. 1263–1279
- [11] He J.H., Liu Y.: 'Control of bubble size and bubble number in bubble electrospinning', *Comput. Math. Appl.*, 2012, **64**, (5), pp. 1033–1035
- [12] Qiang J., Wan Y.Q., Yang L.N., *ET AL.*: 'Effect of ultrasonic vibration on structure and performance of electrospun PAN fibrous membrane', *J. Nano. Res.*, 2013, **23**, (35), pp. 96–103